Materials Science & Engineering A 559 (2013) 14–21

Contents lists available at SciVerse ScienceDirect

Materials Science & Engineering A

journal homepage: www.elsevier.com/locate/msea

A comparative study of pulsed Nd:YAG laser welding and TIG welding of thin Ti6Al4V titanium alloy plate

Xiao-Long Gao, Lin-Jie Zhang *, Jing Liu, Jian-Xun Zhang

State Key Laboratory of Mechanical Behavior for Materials, Xi'an Jiaotong University, Xi'an 710049, China

ARTICLE INFO

Article history:
Received 21 December 2011
Received in revised form
2 May 2012
Accepted 4 June 2012
Available online 4 July 2012

Keywords:
Ti6Al4V titanium alloy
Pulsed Nd:YAG laser welding
TIG welding
Joint properties

ABSTRACT

This paper reports on a study aiming at comparing properties of the Ti6Al4V titanium alloy joints between pulsed Nd:YAG laser welding and traditional fusion welding. To achieve the research purpose, Ti6Al4V titanium alloy plates with a thickness of 0.8 mm were welded using pulsed Nd:YAG laser beam welding (LBW) and gas tungsten arc welding (TIG), respectively. Residual distortions, weld geometry, microstructure and mechanical properties of the joints produced with LBW and TIG welding were compared. During the tensile test, with the aid of a high speed infrared camera, evolution of the plastic strain within tensile specimens corresponding to LBW and TIG welding were recorded and analyzed. Compared with the TIG, the welded joint by LBW has the characters of small overall residual distortion, fine microstructure, narrow heat-affected zone (HAZ), high Vickers hardness. LBW welding method can produce joints with higher strength and ductility. It can be concluded that Pulsed Nd:YAG laser welding is much more suitable for welding the thin Ti6Al4V titanium alloy plate than TIG welding.

1. Introduction

Due to its low density, excellent high temperature mechanical properties and good corrosion resistance, Ti6Al4V titanium alloy has been widely used in the aerospace, automotive, petrochemical, nuclear and power generation industries. With the development of titanium industries, many welding methods such as TIG welding, laser beam welding, laser hybrid welding, electron beam welding (EBW), friction welding have already been developed [1–10].

Up to now, TIG welding is one of the most widely used welding methods for titanium alloy, particularly in sheet form [11]. A main drawback of TIG welding is its high heat input and the resulted greater distortion and higher risk of contamination [12]. At temperatures exceeding 500 °C, Ti6Al4V titanium alloy is highly susceptible to absorb harmful gas and, as a result, problems such as poor mechanical properties and unstable structure would be induced. Therefore, many studies on the influence of welding method difference on the performance of titanium alloy joint have been published. It was reported that, compared to the joint welded by TIG or EBW, titanium alloy joint welded by LBW has many advantages such as narrower weld-seam and fine grains [13]. Li et al. [14] did a comparative study of laser beam welding and laser/MIG hybrid welding (LAMIG) of Ti–Al–Zr–Fe titanium alloy. They found that both the joint produced by LBW and that produced by LAMIG fractured at the parent metal, while LAMIG welded joints presented higher bending angles in face bending test. Zhang's work revealed that residual stress distribution in a titanium alloy joint welded by LBW is similar to that obtained from a joint welded by traditional fusion welding method, although the distribution zone is much narrower when LBW was used [15].

Pulsed Nd:YAG laser welding is characterized by periodic heating of the workpiece by intermittent pulsed laser power, which allows melting and solidification to take place consecutively [16]. And, therefore, more precise control of heat input becomes available in pulsed Nd:YAG laser welding. Compared with conventional welding method, pulsed Nd:YAG laser welding usually provides benefits such as lower heat input, less deformation, narrower weld bead and narrower heat affected zone [17,18]. The solidification time in pulsed Nd:YAG laser is even shorter than that in a continuous laser beam welding or electron beam welding. Hence, it should be expected that pulsed Nd:YAG laser is much more feasible for welding thin Ti6Al4V titanium alloy sheets.

In this work, in order to get a better understanding of the influence of the pulsed Nd:YAG laser welding and traditional fusion welding method on the properties of Ti6Al4V joints, Ti6Al4V sheets with a thickness of 0.8 mm were welded with pulsed Nd:YAG laser and TIG arc, respectively. The influence of methods difference on the weld geometry, residual distortion, microhardness, microstructure and mechanical properties were studied systematically.

2. Experimental materials and methods

In this study, butt welding experiments were carried out on commercial mill-annealed Ti6Al4Vtitanium alloy sheets with a dimension of 260 × 110 × 0.8 mm using JHM-1GXY-400X pulsed

* Corresponding author. Tel.: +86 29 82663115; fax: +86 29 82668807.
E-mail address: zhanglinjie@mail.xjtu.edu.cn (L.-J. Zhang).

0921-5093/$ - see front matter © 2012 Elsevier B.V. All rights reserved.
http://dx.doi.org/10.1016/j.msea.2012.06.016

Table 1
Chemical compositions of Ti6A4V titanium alloy and TC-1 welding wire (wt.%).

	Ti	Al	V	Mn	Fe	Si	C	N	H	O
Ti6Al4V	Balance	5.5–6.8	3.5–4.5	–	< 0.3	< 0.15	< 0.1	< 0.04	< 0.015	< 0.15
TC-1	Balance	1.81	–	0.73	0.02	–	0.006	0.013	0.0006	–

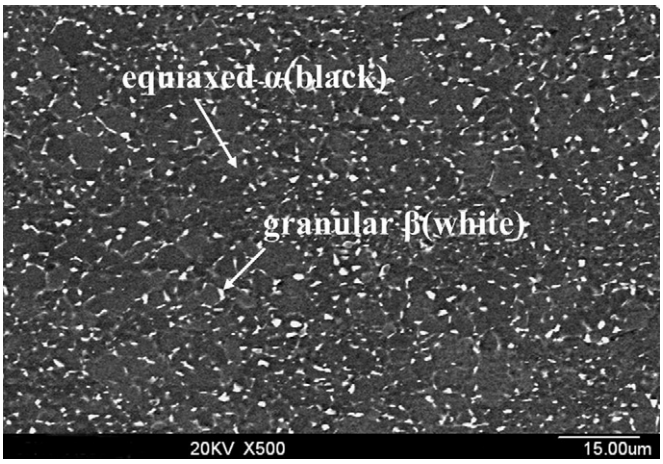

Fig. 1. Microstructure of Ti6Al4V.

Table 2
Welding parameters of LBW and TIG.

Current	Pulse duration	Pulse frequency	Welding speed	Focal position (mm)
Welding parameters				
LBW				
150 A	5.5 ms	20 Hz	600 mm/min	−2 mm
Voltage	Current	Pulse frequency	Welding speed	Focal position (mm)
Welding parameters				
TIG				
10 V	30 A	–	20 mm/min	–

Nd:YAG laser and TIG arc, respectively. The chemical composition of Ti6Al4V is shown in Table 1. As is shown in Fig. 1, the base metal (BM) consists of the black equiaxed α and the white granular β. In the TIG welding process, filler wire was TC-1 with a diameter of 1 mm. The chemical composition of TC-1 is also shown in Table 1. The welding parameters for both LBW and TIG welding are shown in Table 2. The plates are mechanically brushed, acid pickled in an HF solution and cleaned with acetone prior to welding. As titanium alloy is highly reactive with ambient gases, especially at high temperatures, argon was used as shielding gas during both welding processes.

After welding, digital photographs were used to capture the bead appearance. Residual distortion of the welded plates was measured with the aid of a XJTUOM-II dimensional dense point cloud measuring system. Then, the specimens were sectioned transverse to the welding direction, polished and etched with Kroll solution for optical and scanning electron microscope (SEM) microstructure analysis. Vickers microhardness measurements were done on the base metal, heat affected zone (HAZ) and fusion zone (FZ) by a diamond pyramid indenter under a load of 100 g with a dwelling time of 10 s.

In addition, tensile samples with the dimensions shown in Fig. 2 were prepared. Tensile testing was performed at room

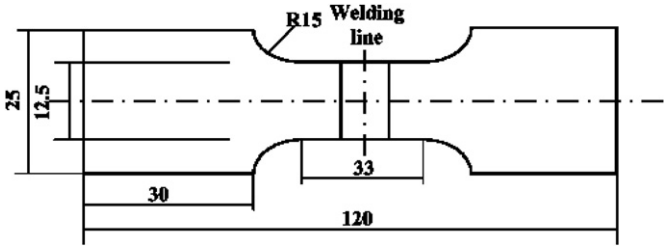

Fig. 2. Dimensions of the tensile specimen (unit: mm).

temperature on CSS-88100 universal tensile test system with a constant drawing speed of 2 mm/min. Before the welded joints were machined, the face and back sides of the weld were minimally ground in order to achieve a smooth surface. During tensile testing, evolution of the sample temperature was captured at a speed of 50 frames per second by a high speed infrared (IR) camera (Vario CAM hr-HS). Spatial resolution and temperature resolution of the infrared camera is 25 μm and 0.03 °C, respectively. After tensile testing, fracture surface morphology of the samples was observed on scanning electron microscopy (SEM).

3. Experimental results and discussions

3.1. Appearance of weld

Fig. 3 shows the front and back bead surface appearance of the joints welded with LBW and TIG methods. It can be seen that both bead formations are smooth and in a bright sliver color. No defects such as oxidation and cracks were found in the joints.

The cross-section profiles of LBW and TIG welded joints are illustrated in Fig. 4. It can be seen from Fig. 4 that both joins were full penetrated and no cracks, porosities or undercuts were found. The top and bottom widths of FZ in LBW joint are 1.32 mm and 0.8 mm, respectively, while those of the TIG welded joint are 4.97 mm and 4.11 mm, respectively. The widths of HAZ at the middle of the LBW and TIG welded joint are 0.34 mm and 2.66 mm, respectively. Due to the larger heat input of TIG welding process, the width of the seam produced by TIG welding is much larger than that of the seam produced by LBW welding. Nevertheless, as melted welding wire can introduce additional liquid metal into the molten pool in TIG welding process, protruding surfaces are observed in TIG welded joint. In the LBW joint, due to the higher welding speed and lower heat input, the size of grain in the FZ of LBW welded joint is the larger size than that of TIG welded joint, even in a relatively low magnification.

3.2. Residual distortion

Fig. 5 shows the residual distortion in cooled down specimens after LBW and TIG welding. Fig. 6 shows the out-of-plane deformation of specimens after LBW and TIG welding measured by a XJTUOM-II dimensional dense point cloud measuring system. It can be seen from Figs. 5 and 6 that the deformation in the plate welded by TIG welding is significantly greater than that in the plate welded by LBW welding. The deformation in the plates can

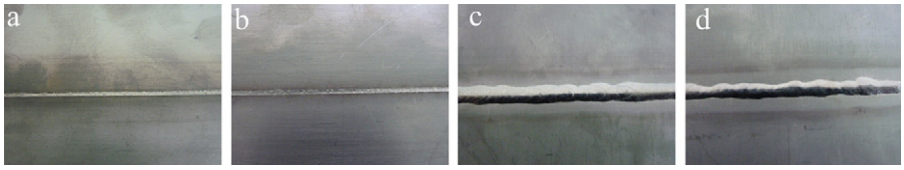

Fig. 3. Surface appearance of Ti6Al4V titanium alloy joints welded by LBW and TIG: (a) front of LBW joint, (b) back of LBW joint, (c) front of TIG joint and (d) back of TIG joint.

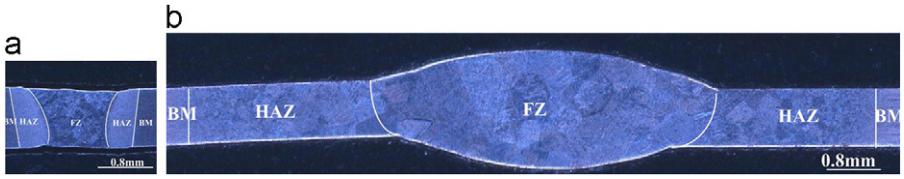

Fig. 4. Cross-section profile of LBW and TIG welded joints: (a) LBW joint and (b) TIG joint.

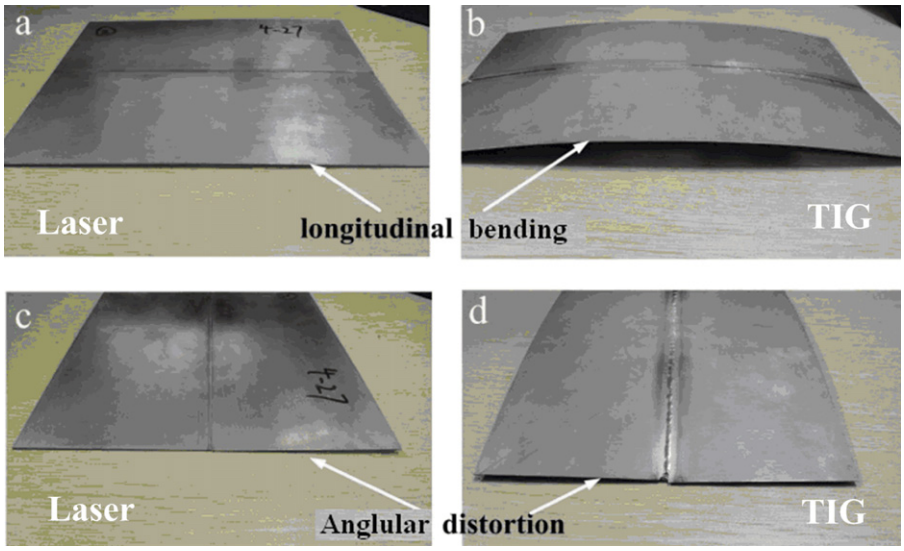

Fig. 5. Distortion pattern of the welded plates: (a) Longitudinal bending of LBW, (b) Longitudinal bending of TIG, (c) Angular distortion of LBW and (d) Angular distortion of TIG.

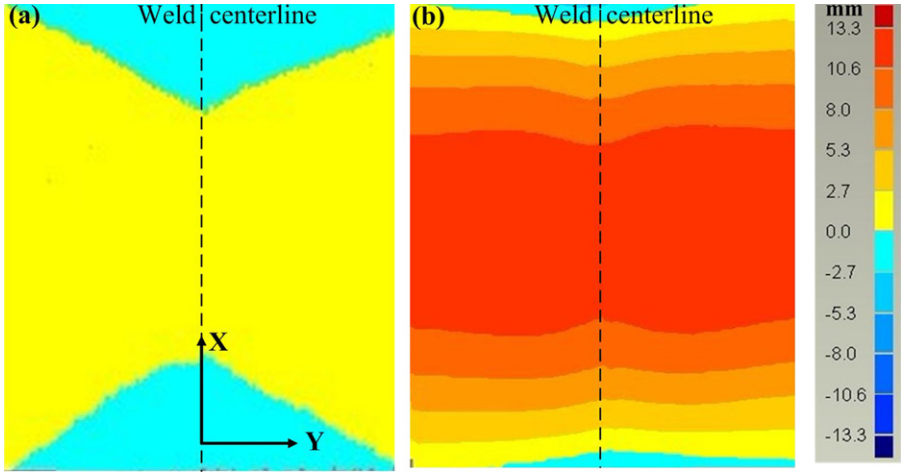

Fig. 6. Measured out-of-plane deformation of plates after LBW and TIG welding.

be separated into two parts, which are the longitudinal bending of the sheet and the angular distortion of the sheet (shown in Fig. 7). As shown in Fig. 6, the distribution of these two kinds of displacement is basically symmetrical against the weld centerline. It can also be seen from Fig. 6 that the maximum longitudinal bending occurs at the longitudinal section with $Y = 0$ mm, while the maximum angular distortion might appear at the igniting end or extinguishing end of the weld. Here, X and Y

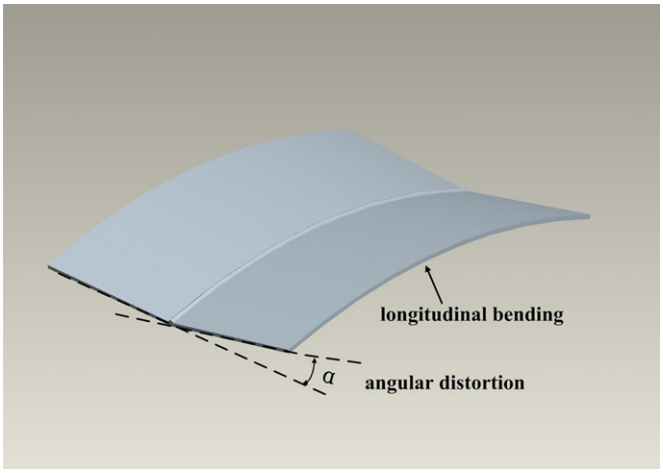

Fig. 7. Schematic of out-of-plane deformation caused by welding.

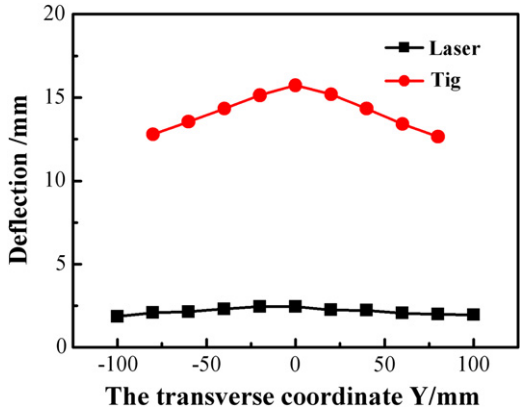

Fig. 8. Comparisons of longitudinal bending between LBW and TIG.

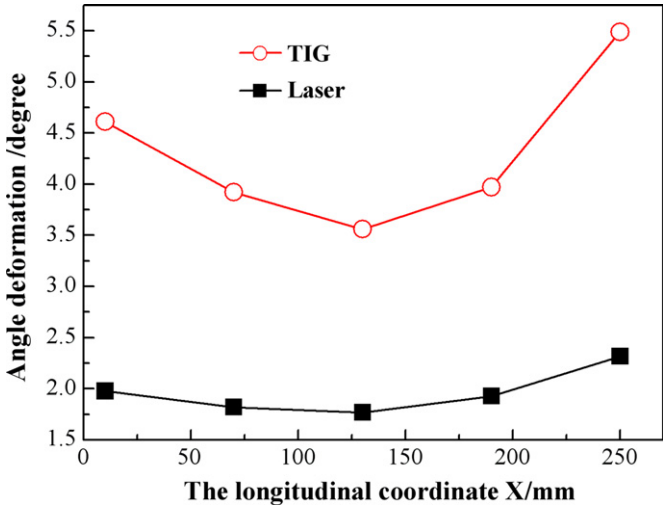

Fig. 9. Comparisons of angular distortion between LBW and TIG.

are the coordinate in *x*-direction and *y*-direction respectively. The coordinate system is shown in Fig. 6a.

Fig. 8 shows the longitudinal profile against the transversal coordinate *Y*. It can be seen from Fig. 8 that the maximum longitudinal bending appeared at the section with $Y = 0$ mm in the TIG welded plate, while the minimum longitudinal bending is at the far edges of the laser welded plate. Similar situation occurs in the LBW welded plate. Arch rise of the profile of longitudinal

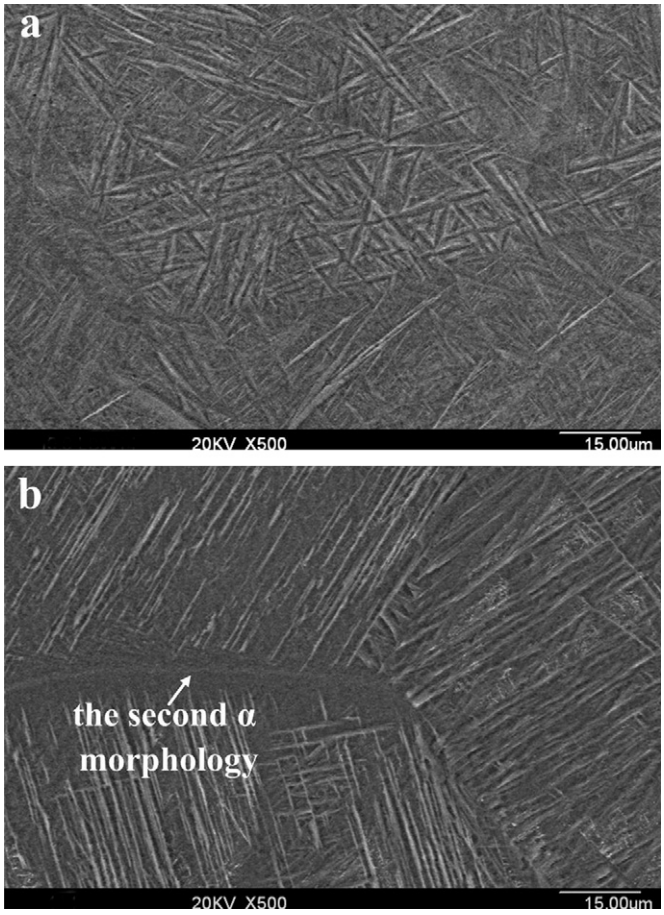

Fig. 10. Microstructures of FZ in the as-welded condition: (a) LBW and (b) TIG.

section with $Y = 0$ mm in the TIG welded plate and the LBW welded plate is 15.7 mm and 2.5 mm, respectively. The probable reason of this bending is that the in-plane expansion of the weld metal are restricted by their adjacent regions and results in compressive plastic strain at the weld zone, and then higher longitudinal shrinkages would be observed in the weld than the outer rim of the plate, as reported by Long et al. [19].

Fig. 9 describes the variation of angular distortion against the longitudinal coordinate *X*. The results in Fig. 9 show that angular distortion induced by TIG welding is much larger than that induced by LBW welding. In addition, it can be seen from Fig. 9 that angular distortion at the extinguishing end of the weld is larger than that at the igniting end of the weld, and the minimum angular distortion would appears at about the middle of the weld. The maximum angular distortion of TIG welded plate and LBW welded plate are 5.5° and 2.3°, respectively.

3.3. Structure of welding joints

Fig. 10 compares the microstructures of FZ in the as-welded condition between LBW welded joint and TIG welded joint. We found that a fully acicular α′ solidification structure was observed in the FZ of LBW welded joint, as shown in Fig. 10a. In the weld zone of TIG welded joint, due to the relatively lower cooling rate, the microstructure consists of acicular α′ and some second α morphology at the boundaries of prior β, as shown in Fig. 10b. The cooling rate is always above the critical cooling rate of 410 °C/s which allows the formation of a full acicular martensitic α′ structure, while at slightly lower cooling rates (410 °C/s) the transformed α phase is preferential to form at prior β grain

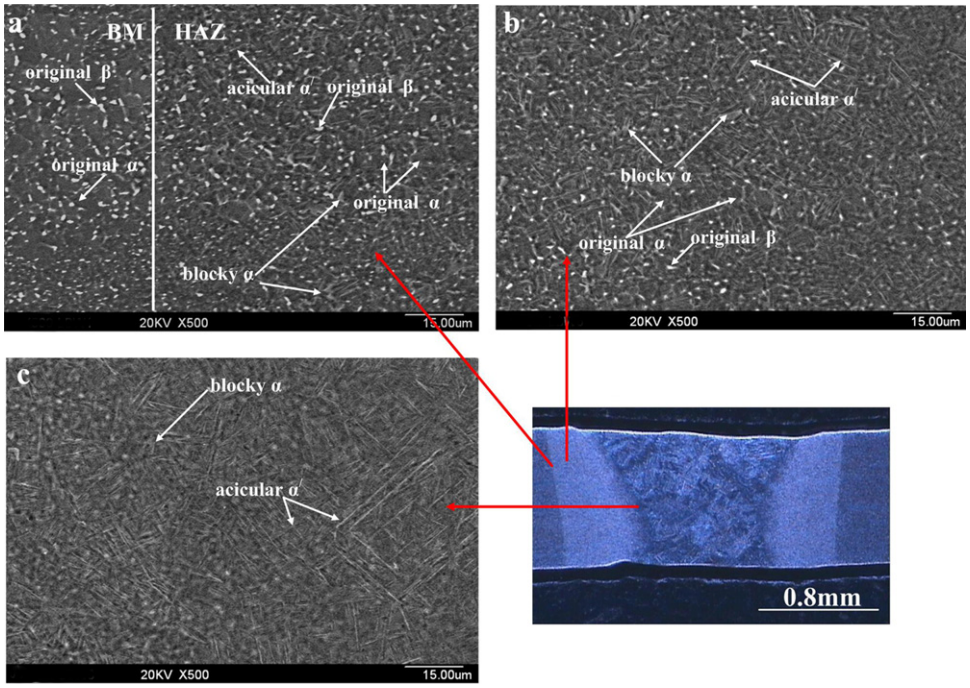

Fig. 11. Microstructure of the HAZ of LBW joint.

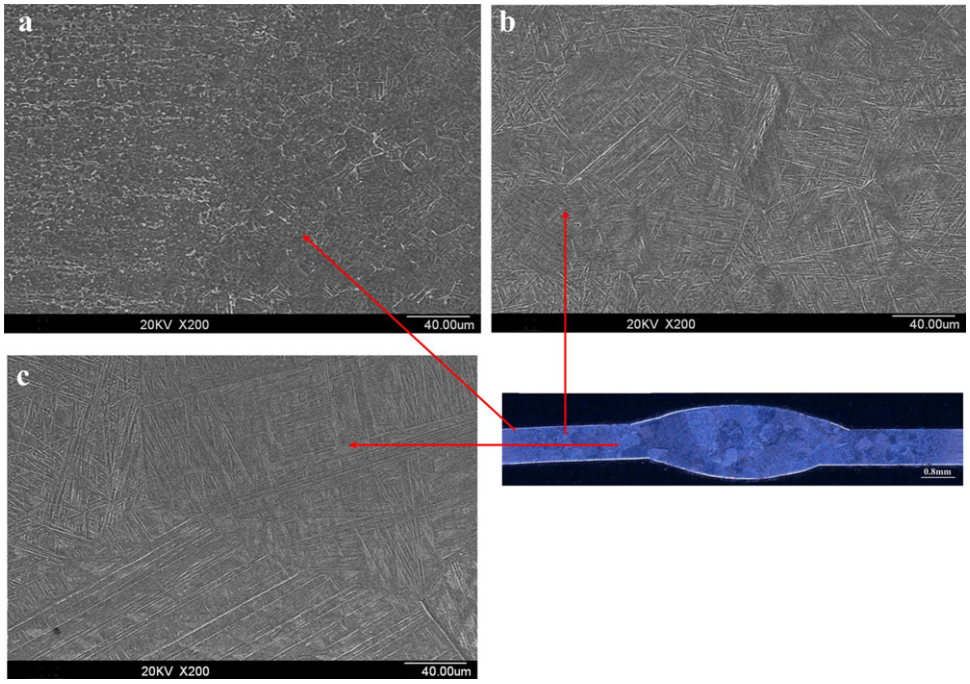

Fig. 12. Microstructure of the HAZ of TIG joint.

boundary in Ti–6Al–4V [20]. It is indicated that the cooling rate in the LBW welding is greater than that in the TIG.

Figs. 11 and 12 show the microstructure of HAZ of LBW welded joint and TIG welded joint, respectively. As shown in Fig. 11, the HAZ near the BM is complicated, which consists of acicular α′ phase, the blocky α phase (transformed α phase), original α phase and β phase. However, the HAZ near the FZ is made up of the blocky α phase and the acicular α′ phase. The acicular α′ phase, the blocky α phase, original α phase and β phase have been found in the HAZ of Ti6Al4V alloy during laser welding by Fan et al. [21] and Liu et al. [22]. The HAZ near the BM can be considered to be the partially transformed region due to the appearance of the original α phase and β phase. But the original α phase and the original β phase are not found in the HAZ near the FZ, and thus the region can be considered to be the fully transformed region. With the aid of the *situ* time-resolved X-ray diffraction (TRXRD) during the TIG welding, the partially and fully transformed regions of HAZ in the weld of Ti–6Al–4V by TIG have been observed by Elmer et al. [23]. Compared with TIG welding, the partially and fully transformed regions of HAZ during laser welding are more likely to appear because of lower heat input. The partially and fully transformed regions of HAZ in the weld of

Ti6Al4V alloy by LBW have been determined by Liu et al. [22]. From Fig. 11, it is also observed that the content of acicular α′ is decreased significantly from the region near the FZ to region near the BM, which would cause the great gradient of α′ content in the narrow HAZ. Similar α′ gradient was observed by Squillace et al. [24] and Cao and Jahazi [25]. From Fig. 12, it can be seen that microstructure of the HAZ of TIG welded joint consists of martensitic α′ and α phase within prior β grains. The much smaller β grains of the HAZ are more or less equiaxed and decrease in size from with increasing distance from the weld centerline. There is a gradient of prior β grain sizes extending from the HAZ/FZ boundary to the region of BM/HAZ boundary. Compare with LBW welding, the variations microstructure from the FZ to the HAZ near the FZ for TIG welded joint is few. This can be explained by the larger heat input and less temperature gradients of TIG welding process [26], which determines the microstructure evolution. In addition, a comparison between Figs. 11 and 12 reveals that the size of crystals in HAZ was greatly reduced when LBW welding method was employed.

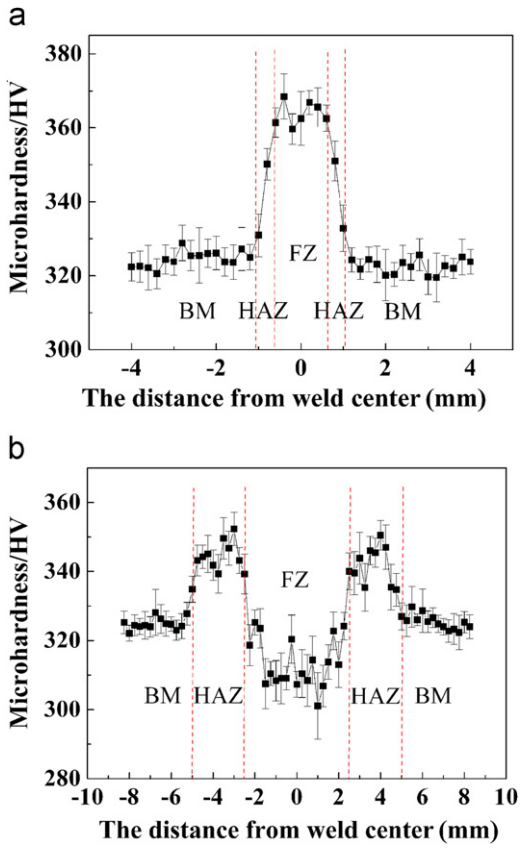

Fig. 13. Microhardness distribution on the cross-section of LBW and TIG welded joints: (a) LBW and (b) TIG.

Fig. 14. A view of butt joints welded by LBW and TIG after tensile tests.

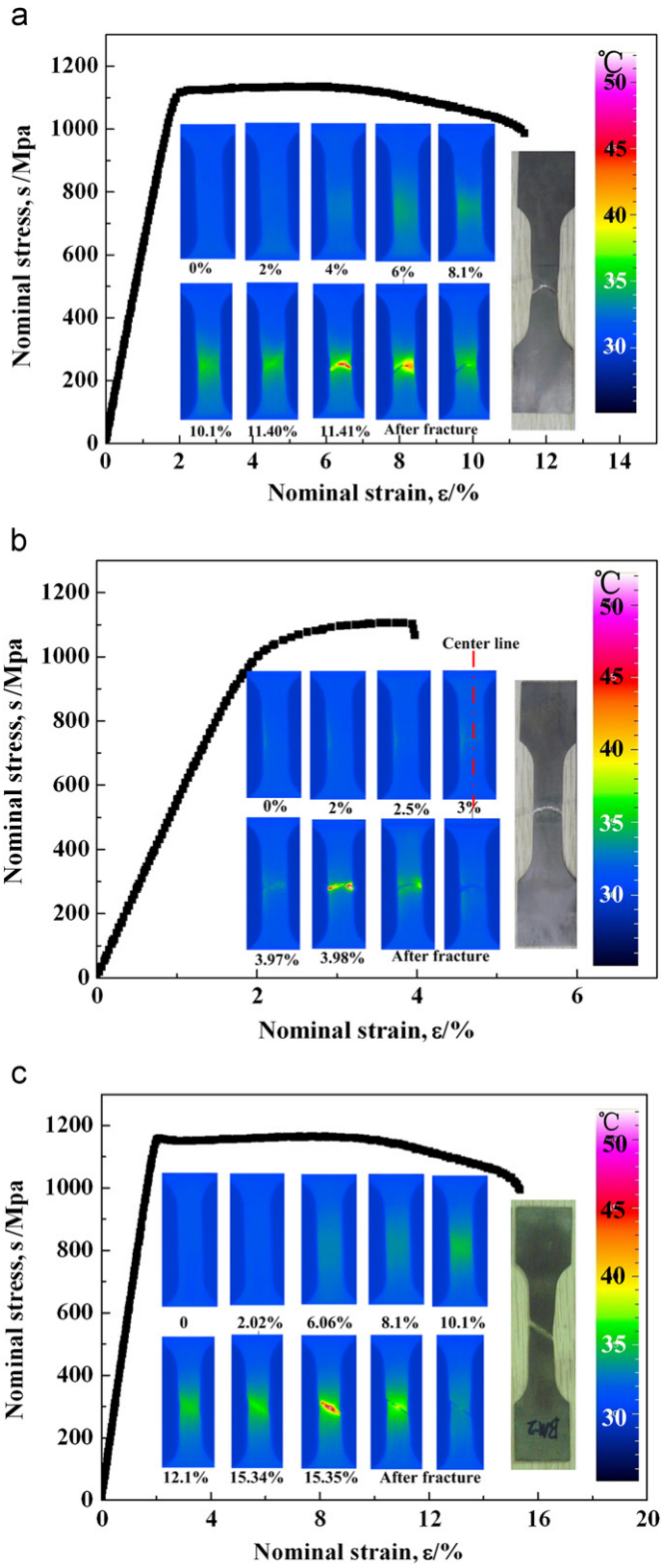

Fig. 15. Infrared thermography images sequence during tensile loading: (a) the specimen by LBW, (b) the specimen by TIG and (c) the specimen of BM.

3.4. Mechanical properties

Fig. 13 shows the microhardness distribution on the cross-section of the LBW and TIG welded joint. As shown in Fig. 13a, the FZ in the LBW welded joint exhibits the highest hardness due to the formation of the martensite α′, then the hardness values drop rapidly in the HAZ of LBW welded joint. The average hardness of BM is approximate 324HV, while the average hardness in the FZ of LBW welded joint is 364HV. Since the HAZ width of LBW welded joint is very narrow, the hardness gradient in the HAZ is rather large, which implying the serious heterogeneity of mechanical properties over the narrow HAZ of LBW welded joint. In TIG welded joints, the average hardness of FZ and HAZ is 311HV and 342HV respectively. The microhardness in the fusion zone of TIG welded joint is much lower than that of BM. The reason may be the low strength-index filler wire used in the TIG welding process. In addition, it can also be seen from Fig. 13 that microhardness gradient in the HAZ of TIG welded joint is less than that of LBW welded joint.

Shown in Fig. 14 are the tensile test results of LBW welded joint and TIG welded joint. It was found that the joint welded by LBW fractured at the parent metal, while the joint welded by TIG fractured at the FZ. The tensile strength (σ_b) for the joint welded by LBW and that welded by TIG are 1134MP and 1105 MPa, respectively. Lower tensile strength (σ_b) of the joint welded by TIG can be explained by that low strength-index TC-1 wires was used in TIG welding process.

Fig. 15 illustrates the evolution of nominal stress and the typical thermal sequences of the specimen during tensile testing for the LBW welded joint, TIG welded joint and parent metal. From the results shown in Fig. 15, it can be seen that temperature change during the elastic stage of deformation is negligible for all these three kinds of specimen. When the loaded specimen is stressed in some area above its yield limit, plastic dissipation occurs and a major portion of the plastic work is released as heat. Since the plastic dissipation is always positive, it would cause a temperature rise within the loaded specimen. Therefore, infrared thermographs shown in Fig. 15 can be used to evaluate the impacts of welding method difference on the evolution of the plastic stain within a specimen during tensile test. A glance at Fig. 15 reveals that the temperature distribution in the specimens exhibits a characteristic of heterogeneity, which provides evidences of heterogeneous plastic strain in the specimen [27]. Furthermore, during tensile tests, the evolution of plastic strain in the three kinds of specimen is quite different. It seemed that strongly localized plastic strain firstly occurred in the specimen welded by TIG due to that low strength-index TC-1 wires was used in the TIG welding process, while the BM specimen with uniform structure and mechanical properties took the longest tensile time for the appearance of strongly localized plastic strain. It can be seen from Fig. 15 that a narrow heated zone with a maximum temperature of about 45 °C appeared in the weld zone of TIG welded joint at 39.28 s, while the maximum temperature in the LBW welded joint was still less than 35 °C at 40 s. For the BM specimen, the maximum temperature was less than 35 °C until 100 s.

Fig. 16 shows the stress–time curves and the ΔT–time curves. Here, ΔT is the span of temperature along the central line (as given in Fig. 15b) of the specimen, which equals to the remains after the minimum temperature along the central line of specimen is subtracted from the maximum temperature along the central line of specimen. The location of specimen center line is shown in Fig. 15b. It can be seen from Fig. 16 that the span of temperature along the specimen center line increases with the increasing of tensile time, which indicates plastic strain heterogeneity increases with the increasing of tensile time. In addition, it was found that the ΔT of parent metal is always less than that of the other two kinds of specimen. This is due to that both LBW joint and TIG joint are heterogeneous in microstructures and mechanical properties, which would result in strongly localized plastic strain during the tensile test.

Fracture surfaces of the tensile specimens were examined by SEM. Shown in Fig. 17a–c are the fracture surface morphologies of BM, LBW welded joint and TIG welded joint, respectively. Specimen of LBW welded joint fractured in parent metal, while the TIG welded joint is broken in FZ. On the fracture surfaces of BM and LBW welded joint, numerous dimples can be found, indicating that both specimens are subjected to large plastic deformation prior to failure. Hence, the failure of BM and LBW welded joint is due to ductile fracture. The fracture surface of TIG welded joint exhibited a feature of dominant dimple fracture appearance combined with cleavage fracture appearance, indicating the lower ductility of the FZ. The reasons might be the coarse structure observed in the weld zone of TIG welded joint, as shown in Fig. 4.

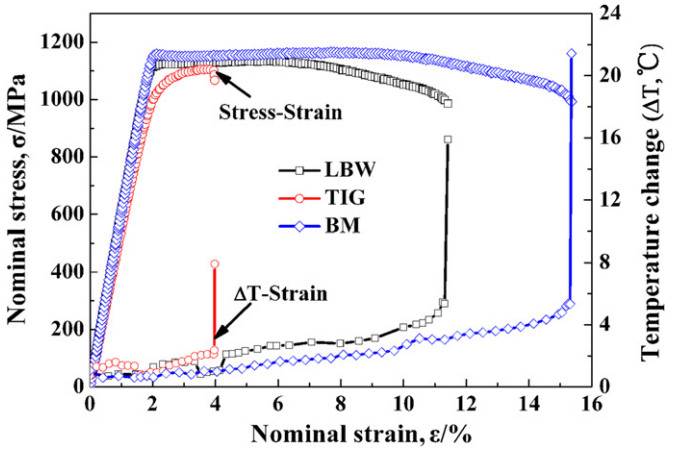

Fig. 16. Time evolution of the span of temperature along the central line of the specimen.

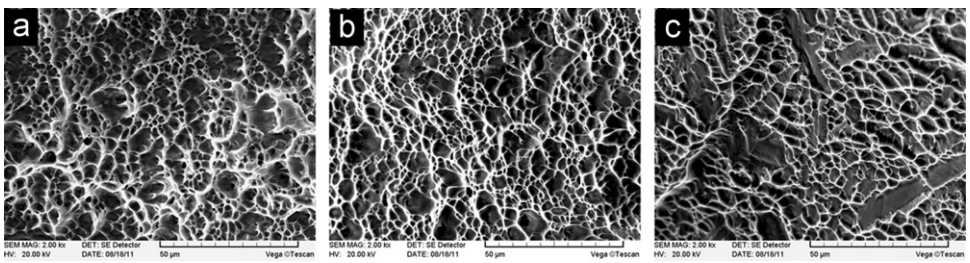

Fig. 17. Morphologies of fracture surface of tensile specimens: (a) BM specimen, (b) LBW (broken in the BM), (c) TIG (broken in the FZ).

4. Conclusions

Based on the above introduced work, we can come to the following conclusions:

1. The FZ width, HAZ width and overall residual distortion of the joint welded by TIG are significantly greater than that of the joint welded by LBW.
2. The microstructure at the fusion zone of the TIG welded joint consists of acicular α' and little the second α morphology, while that of the joint welded by LBW fully consists of acicular α' due to the large cooling rate in laser welding process.
3. The results of high speed infrared imaging indicate that strongly localized plastic strain firstly occurred in the specimen by TIG due to that low strength-index TC-1 wires was used in the TIG welding process, while the BM specimen with uniform structure and mechanical properties took the longest tensile time for the taking place of strongly localized plastic strain.
4. The LBW welded joints have better combination of strength and ductility. The process of the LBW welding is proved to be much more feasible for the production of titanium plate joints.

Acknowledgements

The authors wish to thank Professor Jiang-Tao Xiong from Northwestern Polytechnical University for his valuable comments and advices. This work was supported by National Natural Science Foundation of China (Grant No. 50875200), Research Fund for the Doctoral Program of Higher Education of China (Grant Nos. 20100201110065 and 20090201120014), Natural Science Foundation of Shaanxi Province (Grant No. 2011JM6008) and Fundamental Research Funds for the Central University of China.

References

[1] M. Balasubramanian, V. Jayabalan, V. Balasubramanian, Mater. Lett. 62 (6–7) (2008) 1102–1106.
[2] W. Zhou, K.G. Chew, Mater. Sci. Eng. A347 (2003) 180–185.
[3] J.E. Blackburn, C.M. Allen, P.A. Hilton, L. Li, M.I. Hogue, A.H. Khan, Sci. Technol. Weld. Join. 15 (5) (2010) 433–439.
[4] Z. Li, S.L. Gobbi, I. Norris, S. Zolotovsky, K.H. Richter, J. Mater. Process. Technol. 65 (1) (1997) 203–208.
[5] L. Cui, K. Muneharua, S. Takao, Mater. Des. 30 (1) (2009) 109–114.
[6] P.E. Denney, B.W. Shinn, P. Mike Fallara, in: Proceedings of the 15th International Offshore and Polar Engineering Conference, Seoul, Korea, June 19–242005, pp. 106–108.
[7] J.L. Barreda, F. Santamaria, X. Azpiroz, A.M. Irisarri, J.M. Varona, Vaccum 62 (2–3) (2001) 143–150.
[8] N. Saresh, M.G. Pillai, J. Mathew, J. Mater. Process. Technol. 192–193 (2007) 83–88.
[9] Y. Zhang, Y.S. Sato, H. Kokawa, S.H. Park, S. Hirano, Mater. Sci. Eng. A 485 (2008) 448–455.
[10] L. Zhou, H.J. Liu, Q.W. Liu, Mater. Des. 31 (5) (2010) 2631–2636.
[11] W.A. Baeslack III, J.M. Gerken, C. Cross, J. Hanson, P.S. Liu, J.C. Monses, J. Schley, L. Showalter, 8th edition,Welding Handbook, vol. 4, American Welding Society, Miami, FL, USA, 1998, pp. 488–540.
[12] S. Lathabai, B.L. Jarvis, K.J. Barton, Mater. Sci. Eng. A 299 (2001) 81–93.
[13] Q. Yunlian, D. Ju, H. Quan, Z. Liying, Mater. Sci. Eng. A 280 (2000) 177–181.
[14] R. Li, Z. Li, Y. Zhu, R. Lei, Mater. Sci. Eng. A 528 (2011) 1138–1142.
[15] J.X. Zhang, Y. Xue, S.L. Gong, Sci. Technol. Weld. Join. 10 (6) (2005) 643–646.
[16] F. Malek Ghaini, M.J. Hamedi, M.J. Torkamany, J. Sabbaghzadeh, Scr. Mater. 56 (11) (2007) 955–958.
[17] Y.F. Tzeng, Int. J. Adv. Manuf. Technol. 16 (1) (2000) 10–18.
[18] A.V. Vicente, R.B. Jose, R. Wagner, J. Mater. Process. Technol. 210 (14) (2010) 1838–1843.
[19] H. Long, D. Gery, A. Carlier, P.G. Maropoulos, Mater. Des. 30 (10) (2009) 4126–4135.
[20] T. Ahmed, H.J. Rack, Mater. Sci. Eng. A243 (1998) 206–211.
[21] Y. Fan, P. Cheng, Y. Yao, Z. Yang, K. Egland, J. Appl. Phys. 98 (1) (2005) 013518–013518.10.
[22] H. Liu, K. Nakata, N. Yamamoto, J. Liao, J. Mater. Sci. 47 (3) (2012) 1460–1470.
[23] J.W. Elmer, T.A. Palmer, S.S. Babu, W. Zhang, T. DebRoy, J. Appl. Phys. 95 (12) (2004) 8327–8339.
[24] A. Squillace, U. Prisco, S. Ciliberto, A. Astarita, J. Mater. Process. Technol. 212 (2) (2012) 427–436.
[25] X. Cao, M. Jahazi, Opt. Lasers Eng. 47 (11) (2009) 1231–1241.
[26] H.T. Lee, C.T. Chen, J.L. Wu, J. Mater. Process. Technol. 210 (12) (2010) 1636–1645.
[27] A. Ghorbel, N. Saintier, A. Dhiab, Procedia Eng. 10 (2011) 2123–2128.